textiles

MDPI

Article

Electrospun Fe_3O_4-PVDF Nanofiber Composite Mats for Cryogenic Magnetic Sensor Applications

Tonoy Chowdhury [1], Nandika D'Souza [1,2,*] and Diana Berman [2]

[1] Department of Mechanical Engineering, University of North Texas, Denton, TX 76207, USA; tonoychowdhury@my.unt.edu
[2] Department of Material Science and Engineering, University of North Texas, Denton, TX 76207, USA; diana.berman@unt.edu
* Correspondence: ndsouza@unt.edu

Abstract: Magnetically responsive, mechanically stable and highly flexible iron (III) oxide-polyvinylidene fluoride (Fe_3O_4-PVDF) piezoelectric composite fiber mats were fabricated via one step electrospinning method for magnetic sensing at cryogenic temperature. The properties of Fe_3O_4-PVDF composite fiber mats were characterized using scanning electron microscopy (SEM), differential scanning calorimetry (DSC), X-ray diffraction (XRD), Fourier transform infrared (FT-IR) spectroscopy, d_{33} and magnetization test. The fiber diameter decreased as the concentration of Fe_3O_4 increased. The DSC results suggested a decrease in the crystallinity of the composite fiber mats after adding Fe_3O_4, and the XRD curves identified that the decrease in crystallinity took place in the β crystalline phases of the fibers. FT-IR results further confirmed the reduction of β phases of the composite fiber mats which dropped the piezoelectric response of the fiber mats by 38% for 5% Fe_3O_4-PVDF than PVDF fiber but still 400% higher than PVDF pellets. The magnetization test advocated a superparamagnetic state of the fiber at room temperature but a ferromagnetic behavior at a lower temperature. The coercivity values of the mats suggested a homogeneous dispersion of the Fe_3O_4 nanoparticles into the PVDF matrix. Young's modulus (E) of the fibers remained the same before and after the magnetization test, indicating the mechanical stability of the fiber in the range of 5 K to 300 K. Its mechanical stability, superparamagnetic behavior at room temperature and ferromagnetic at low temperature could open up its application in spintronic devices at cryogenic temperature and cryogenic power electronic devices.

Keywords: magnetic sensor; piezoelectric; cryogenic; PVDF; Fe_3O_4; hysteresis

check for updates

Citation: Chowdhury, T.; D'Souza, N.; Berman, D. Electrospun Fe_3O_4-PVDF Nanofiber Composite Mats for Cryogenic Magnetic Sensor Applications. *Textiles* **2021**, *1*, 227–238. https://doi.org/10.3390/textiles1020011

Academic Editors: Raul Fangueiro and Luciano Tarricone

Received: 22 May 2021
Accepted: 20 July 2021
Published: 27 July 2021

Publisher's Note: MDPI stays neutral with regard to jurisdictional claims in published maps and institutional affiliations.

Copyright: © 2021 by the authors. Licensee MDPI, Basel, Switzerland. This article is an open access article distributed under the terms and conditions of the Creative Commons Attribution (CC BY) license (https://creativecommons.org/licenses/by/4.0/).

1. Introduction

Magnetically responsive flexible fabrics are a growing need for shielding electromagnetic interference especially in microelectronic applications to reduce growing electromagnetic pollution, sheaths for portable electronics and stealth weapon systems in military applications [1,2]. These flexible fabrics are also useful for different biomedical applications like magnetic cell separation membranes [3], magnetic resonance imaging contrast agents [4], etc. Their application could also be extended to spintronics and power electronic devices at extremely low temperatures [5,6]. Iron (III) oxide (Fe_3O_4) nanoparticles are a valuable additive because of their electronic, magnetic, optical, and mechanical properties [7]. Composite nanofibers/thin films consisting of magnetic nanoparticles have been under intensive investigation in the last few years [7]. There remains a need to create flexible processable magnetically responsive and mechanically rugged films.

PVDF is a widely used piezoelectric semi-crystalline polymer with five different crystalline phases (α, β, δ, γ and ε) [8,9]. Its piezoelectric properties are directly related to its crystal phases [10]. Nonpolar α and polar β phase are the most common crystalline structures of PVDF where the β phase is responsible for the piezoelectric properties. Thereby, increasing β phase with eliminating α phase content in PVDF was a major area of focus

for the last decade. Cold-drawing (stretching) [11], high-pressure quenching [12], and poling (applying a high electric field) of PVDF [13] were such processes to increase β phase. Electrospinning is another optional simple one-step method for fabricating PVDF nanofibers under a high electric field which converts the α phase into the β phase [14,15]. The high voltage that is involved in this process, boosts up the β phase of the fibers [16]. Moreover, electrospun fibers mats are highly flexible and mechanically strong compare to the solvent cast films [17].

Different filler materials have been introduced into the PVDF matrix for different functional properties such as Fe_3O_4, $MnFe_2O_4$ and $MgFe_2O_4$ for magnetic properties; graphene oxide, CNT for conductive properties, $BaTiO_3$, $PbTiO_3$, $KNbO_3$ for piezoelectric properties [18]. Researchers prepared Fe_3O_4-PVDF nanocomposites films by solvent casting method. Porous systems have been produced using the phase inversion approach [19–22]. According to their reports, the magnetic property of Fe_3O_4-PVDF nanocomposites increased with an increase in Fe_3O_4 loading. However, their limitations were attributed to the poor dispersion of Fe_3O_4 nanoparticles and poor processability. The ruggedness of composites has also been limited at low temperature applications such as spintronics and power electronic devices at cryogenic conditions (<123 K) [5,6]. Thermal stresses paired with low temperature brittleness have been associated with this weakness. Iron oxide has proved valuable as an additive to polymers to increase low temperature retention of strength in aerospace applications [23]. For example, a modified diglycidyl ether of bisphenol-A (DGEBA) epoxy resin reinforced with carbon fiber showed excellent mechanical performance at cryogenic temperature after Fe_3O_4/GO nanofillers were added to it [24]. The filler material (Fe_3O_4/GO) helped the epoxy to retain its mechanical performance at cryogenic temperature.

The objective of this paper is to explore the viability of iron oxide-PVDF as electrospun textiles retaining mechanical and magnetic performance in cryogenic conditions. The effect of the addition of iron oxide on the polymer is explored through the investigation of the crystallinity and piezoelectricity of the composite fiber mats after the addition of Fe_3O_4 nanoparticles into the PVDF matrix. Magnetic response and mechanical properties were evaluated at room temperature and cryogenic temperature (5 K) to see the effect of cryogenic temperature on the performance of the fiber mats.

2. Materials and Methods

PVDF was obtained from Arkema (Kynar® 721, pellet form) with the following properties: density: 1.78 g/cm^3, melt flow index (MFI): 10 g/10 min, tensile strength: 54 MPa, melting temperature: 168 °C. Fe_3O_4 was obtained from SkySpring Nanomaterials Inc. (Houston, TX, USA) with an average particle size of 20–30 nm. Acetone and *N*,*N*-dimethylformamide (DMF) were purchased from Sigma-Aldrich (St. Louis, MO, USA).

2.1. Preparation of Fe_3O_4-PVDF Fiber Mats

Firstly, 18 wt% (*w*/*w*) PVDF was dissolved in DMF/acetone (2:1) solution by stirring at 50 °C for 2 h using a magnetic stirrer in a 250 mL beaker at 200 rpm. After all the pellets dissolved, Fe_3O_4 nanoparticles (1 wt%, 3 wt% and 5 wt% (*w*/*w*) with respect to polymer) were added into the solution. Then, ultrasonication was performed with Sonic Vibracell II (25% pulse amplitude) for 5 min to disperse the Fe_3O_4 nanoparticles in the polymer solution. Next, 5 mL of this electrospinning solution was taken in a syringe and used for electrospinning. The electrospinning parameters were: voltage 15 kV, flow rate 0.05 mL/h, distance 15 cm, and the needle diameter of 0.038 in. At 400 rpm, a spinning roller with nonstick aluminum foil was capturing the fiber. The average thickness of the fabricated fiber mats was 0.1 mm.

2.2. Nanofiber Mats Characterization

Surface morphology of fiber mats was observed via FEI Nova Nano SEM 230 (Thermo Fisher Scientific, Hillsboro, OR, USA). All the samples were sputter coated to reduce the

charge development on their surface. Using a Perkin Elmer DSC6 differential scanning calorimeter, the thermal properties of PVDF and Fe_3O_4-PVDF mats were investigated. The scanning temperature range was 30 °C to 210 °C at a rate of 10 °C per minute. Crystal structures were studied using a Rigaku Ultima III X-ray Diffractometer (Rigaku Americas Corporation, The Woodlands, TX, USA). A Scientific Nicolet 6700 Fourier Transform Infrared (FT-IR) Spectroscopy (Thermo Scientific, Waltham, MA, USA) with an attenuated total reflectance (ATR) detector was used to characterize the functional groups in PVDF and Fe_3O_4-PVDF mats. A d_{33} meter (APC International, Mackeyville, PA, USA) was used to measure the d_{33} value of the fiber. The fiber mats were rolled to make them thick enough for d_{33} testing. The d_{33} testing was done on 5 different spots of the fiber mats and average values were taken. Magnetic properties of the fiber mats were explored by a DynaCool-14 (Quantum Design, San Diego, CA, USA) Physical Properties Measurement System (PPMS) machine. Like in d_{33} testing, fiber mats were rolled and fitted into the coffee straws to do the magnetization testing. The weights of the samples used in the magnetization test were (0.1 ± 0.01) g.

3. Results

3.1. Scanning Electron Microscopy (SEM)

Scanning electron microscopy images of the fibers as a function of iron oxide concentration were analyzed using ImageJ software to calculate the diameter of electrospun fibers. The fiber diameter reduced gradually as the concentration of the Fe_3O_4 increased as shown in Figures 1 and 2. The average fiber diameter reduced up to 26% for 5% Fe_3O_4-PVDF fiber. Similar results were obtained from electrospun PLA and PMMA fibers loaded with Fe_3O_4 nanomaterials [25]. At room temperature, Fe_3O_4 is a conductor material and adding the Fe_3O_4 particles into the PVDF solution increased the dielectric constant of the solution. A higher dielectric constant means higher polarity in the solution as well as a higher ability to stabilize the charges in the Taylor cone which leads to a decrease in nanofiber diameters [26]. O and Fe signals in the EDX chart of the fiber mats, shown in Figure 3, confirmed the presence of Fe_3O_4 in PVDF fiber. Au and Pd picks came from the sputter coated thin conductive film over the samples.

3.2. Differential Scanning Calorimetry (DSC)

The thermal behavior and crystallinity of the fiber mats were studied using the DSC. The results are presented in Figure 4a, where PVDF and all composite electrospun fiber mats showed a similar melting temperature (T_m) at ~160 °C, indicating no disruption in the PVDF thermal transitions. Furthermore, the melting enthalpy of the nanofiber mats was extracted from DSC curves and used to calculate the degree of crystallinity of the fiber mats based on Equation (1):

$$X_c = \frac{\Delta H}{\Delta H^0} \times 100 \quad (1)$$

where X_c is the degree of crystallinity of the fiber mats; ΔH^0 is the melting enthalpy of 100% crystalline PVDF (105 J/g), and ΔH is the melting enthalpy of Fe_3O_4-PVDF meshes. ΔH was corrected by multiplying it with the mass fraction of PVDF in the composite mats. The results, presented in Table 1, indicated a reduction in crystallinity and enthalpy as the magnetite content increases. For 5% Fe_3O_4-PVDF, the crystallinity of the fiber mats decreased by up to 55%. Previous experiments on Fe_3O_4-PVDF films yielded similar findings [14,27]. This may be linked to the partial inhibition effect of Fe_3O_4 addition on polymer crystal formation, similar to inorganic fillers like Al_2O_3, TiO_2, c-$LiAlO_2$, and Sm_2O_3 decreased the crystalline phase of PEO-based polymer electrolyte systems [28–32].

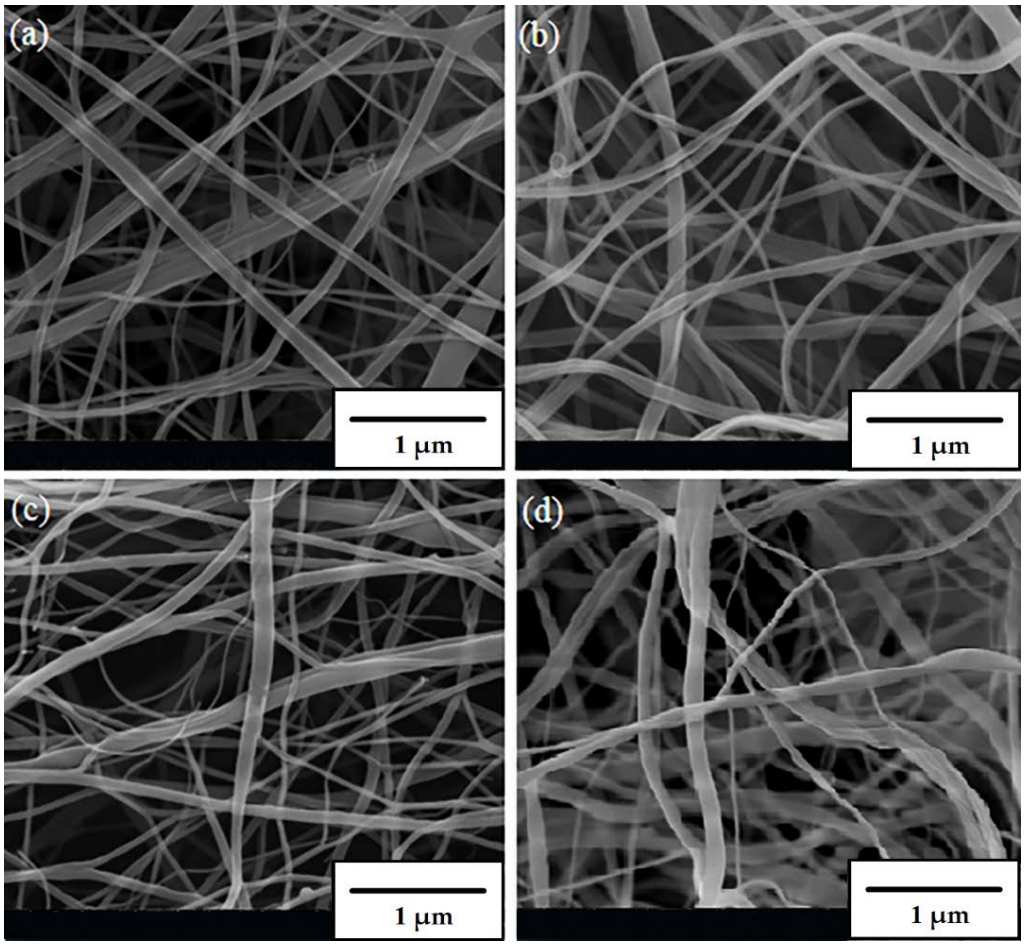

Figure 1. SEM image of (**a**) PVDF (**b**) 1% Fe_3O_4-PVDF (**c**) 3% Fe_3O_4-PVDF and (**d**) 5% Fe_3O_4-PVDF nanofiber mats.

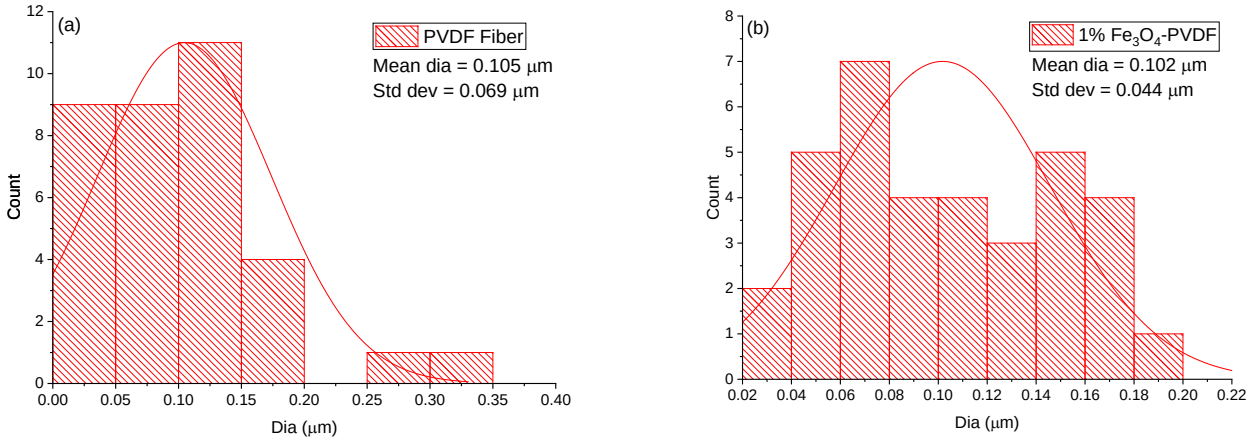

Figure 2. *Cont.*

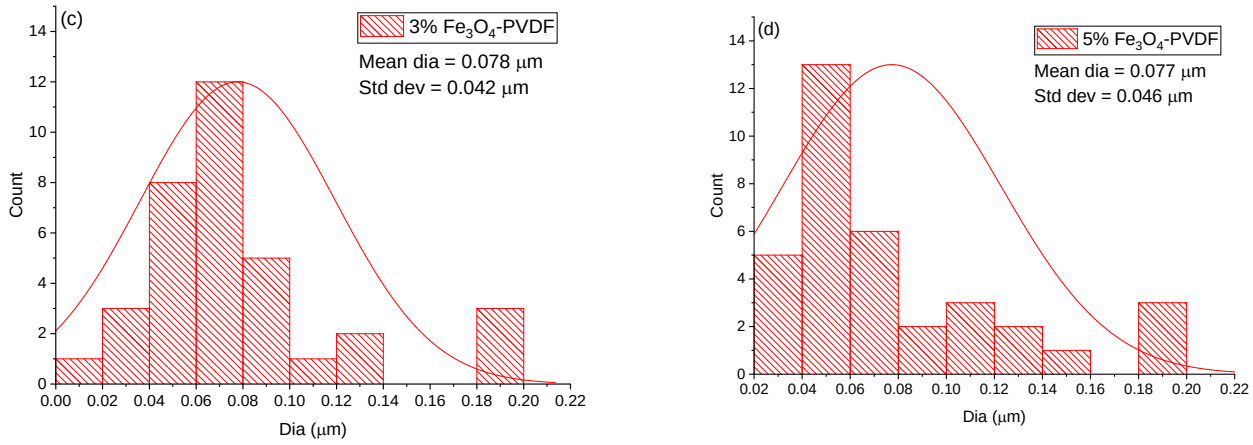

Figure 2. Average fiber diameter for (**a**) PVDF, (**b**) 1% Fe_3O_4-PVDF, (**c**) 3% Fe_3O_4-PVDF and (**d**) 5% Fe_3O_4-PVDF nanofiber mats.

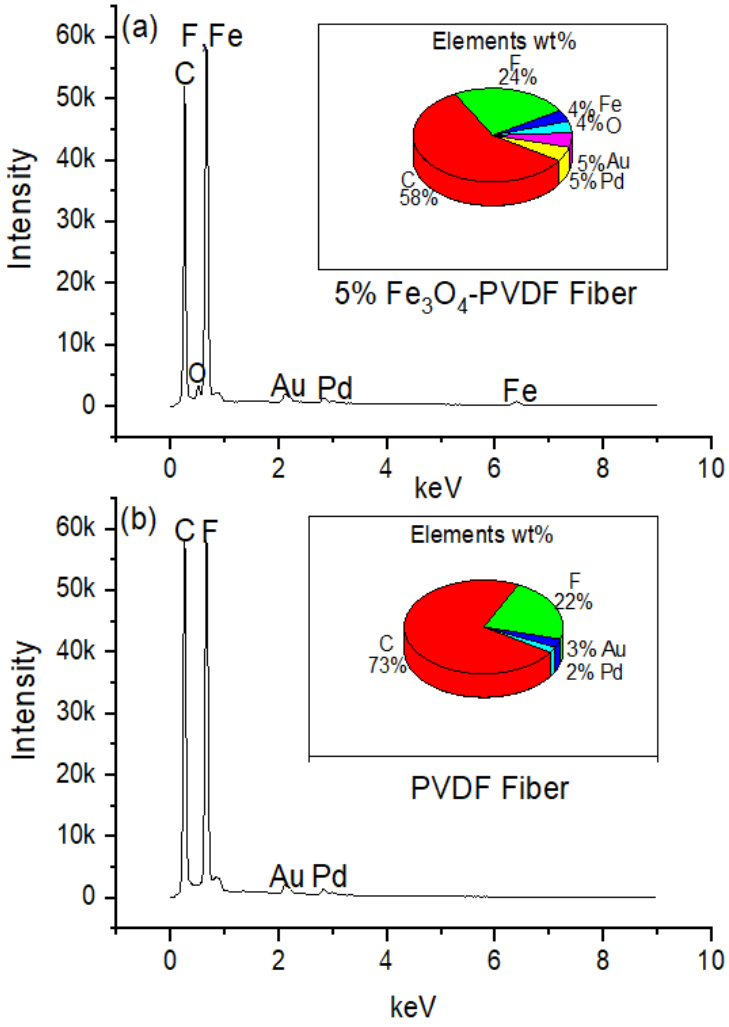

Figure 3. Qualitative EDS analysis of (**a**) 5% Fe_3O_4-PVDF and (**b**) PVDF nanofiber mats.

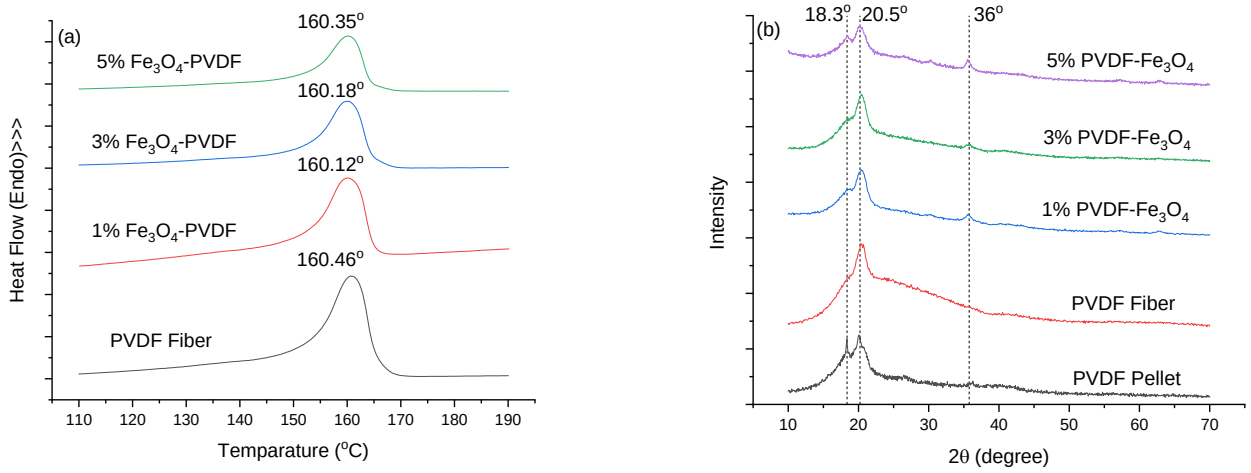

Figure 4. (**a**) DSC curves and (**b**) XRD curves for PVDF and Fe_3O_4-PVDF fiber mats.

Table 1. Enthalpy and percentage crystallinity values obtained from DSC curves.

Sample	T_m (°C)	ΔH (J/g)	Corrected ΔH	X_c (%)
PVDF Fiber	160.12	26.40	26.40	25.14
1% Fe_3O_4-PVDF Fiber	160.46	22.91	22.68	21.81
3% Fe_3O_4-PVDF Fiber	160.35	15.07	14.62	14.35
5% Fe_3O_4-PVDF Fiber	160.18	14.52	13.79	13.82

3.3. X-ray Diffraction (XRD)

The X-ray diffraction (XRD) patterns of PVDF and Fe_3O_4-PVDF nanocomposite fiber mats exhibited strong diffraction peak for all samples at 2θ = 20.5° corresponding to β(110) and β(200) planes, as shown Figure 4b. Weaker diffraction peaks at 36° assigned to β(201) planes were also present [33]. These results indicated that electrospun nanofiber membranes contain mainly β-phase crystal structure of PVDF. Due to the high electric voltage (15 kV) used during the electrospinning method, the random electric dipoles in the PVDF solution aligned, resulting in the forming of the β phase crystal structure. Thereby, the piezoelectric property increased. Also, with increasing loading of the Fe_3O_4 in the polymer matrix, the intensity of the peak at 20.5° decreased (7155, 5634, 4684 and 3401 a.u. for PVDF, 1%, 3% and 5% Fe_3O_4-PVDF respectively). So, the addition of the Fe_3O_4 into PVDF did not promote the crystallization of the PVDF in the β phase. This has been ascribed to inhibition of crystallization by the inorganic particles during the solidification process, which decreases the volume fraction of the crystalline phase in the fiber as discussed in the DSC section [34].

3.4. Fourier-Transform Infrared Spectroscopy (FTIR)

To confirm the XRD results, the authors compared the FTIR spectra of electrospun PVDF nanofiber and Fe_3O_4-PVDF nanofiber mats (Figure 5a). The PVDF pellet exhibited strong peaks at 615 cm^{-1} (CF_2 bending and skeletal bending), 762 cm^{-1} (CF_2 bending), 795 cm^{-1} (CF_2 rocking), and 976 cm^{-1} (CH out-of-plane deformation) which were all recognized as α phase and relatively weak peaks at 840 cm^{-1} (CH_2 rocking), 877 cm^{-1} (CF_2 rocking), 1273 cm^{-1} (CF out-of-plane deformation) and 1402 cm^{-1} (CH_2 scissoring) were considered as β phase [35–37]. Following electrospinning, the α peaks became weaker, while the β crystalline peaks grew stronger. Additionally, the percentage change in β phase can be determined using the following equation (Equation (2)) [35]:

$$F(\beta) = \frac{X_\beta}{X_\alpha + X_\beta} \times 100 = \frac{A_\beta}{1.26A_\alpha + A_\beta} \times 100 \quad (2)$$

where, $F(\beta)$ represents the β phase percentage of PVDF, A_α and A_β are their absorption bands at 763 and 840 cm^{-1}.

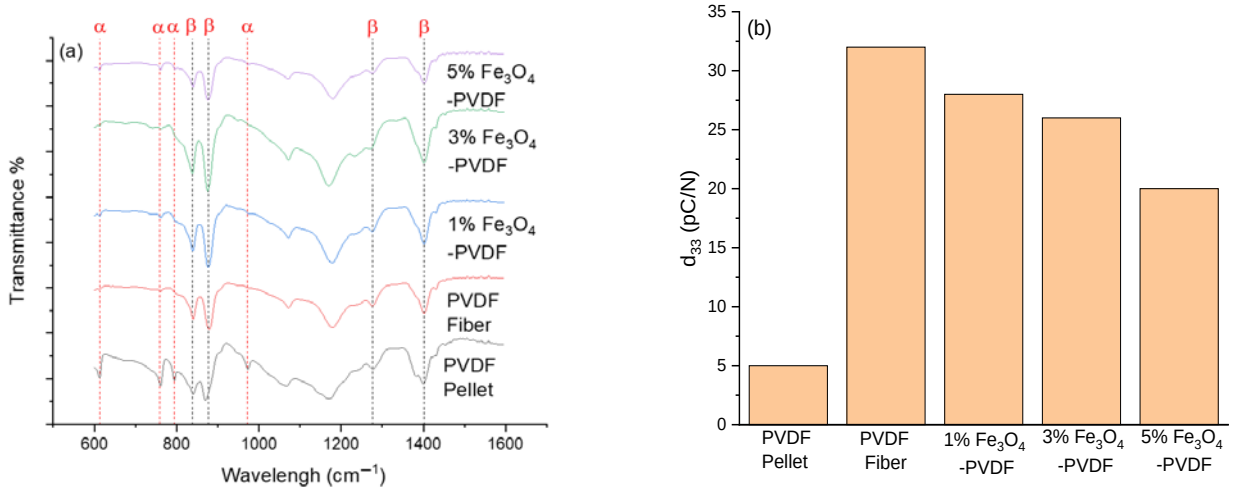

Figure 5. (**a**) FTIR spectra of PVDF and Fe_3O_4-PVDF fibers mats and (**b**) piezoelectric coefficient d_{33} of the fiber mats as a function of Fe_3O_4 mass fraction.

$F(\beta)$ of the PVDF fiber increased significantly by 68% than PVDF pellets due to the electrospinning method as shown in Table 2. With the addition of Fe_3O_4, the β phase decreased slightly compared to the β phase of pure PVDF fiber due to the partial inhibition effect as described in the DSC result discussion section and it kept decreasing as the loading of Fe_3O_4 increasing. The 5% Fe_3O_4-PVDF had the lowest $F(\beta)$ compare to all other electrospun fiber mats but still that value is higher than PVDF pellet by 35%. So, the 5% Fe_3O_4-PVDF should have higher piezoelectric properties than the PVDF pellets which is discussed in d_{33} section.

Table 2. Percentage of beta phase $F(\beta)$ and piezoelectric coefficient (d_{33}).

Sample	$F(\beta)$	d_{33} (pC/N)
PVDF Pellet	48.45 ± 3.43	5 ± 3
PVDF Fiber	81.16 ± 1.81	32 ± 1.73
1% Fe_3O_4-PVDF	73.39 ± 1.24	28 ± 1
3% Fe_3O_4-PVDF	71.69 ± 2.16	26 ± 1
5% Fe_3O_4-PVDF	65.26 ± 3.39	20 ± 2.65

3.5. Piezoelectric Coefficient (d_{33}) Test

The piezoelectric coefficient (d_{33}) of a material specifies the intensity of its piezoelectric effect. The greater the d_{33} value, the more effective the piezoelectric effect [38]. Figure 5b represents the piezoelectric coefficient d_{33} of the PVDF fiber mats as a function of Fe_3O_4 mass fraction. The d_{33} of PVDF mats was 32 pC/N and it dropped gradually to 20 pC/N as Fe_3O_4 increased to a 5% mass ratio. This result was in an agreement with FTIR data. The piezoelectric coefficient d_{33} is directly related to the β phase of the fiber mats. The β phase of the fiber decreased after adding Fe_3O_4 as recorded from FTIR data, which led to the decrease in the d_{33} value. It was also notable that the d_{33} of PVDF pellet was 5 pC/N as recorded in Table 2, whereas the lowest d_{33} value of electrospun fiber mat (5% Fe_3O_4-PVDF) was 20 pC/N; four times higher than PVDF pellets. So, adding Fe_3O_4 might reduce the piezoelectric property of the fiber mats but it has still four times higher piezoelectricity than the PVDF pellet.

3.6. Magnetization Test

M–H measurements were done at 300 and 5 K with the magnetic field varying from −2 T to 2 T (1 T = 10,000 Oe; 1 Oe = 79.577 Am^{-1}) as presented in Figure 6. At 300 K (Figure 6a,b), the samples showed zero coercivity, indicating that the nanofiber mats were in the superparamagnetic state. However, samples showed ferromagnetic behavior at 5 K with a coercivity of ~370 Oe for all the samples as shown in Figure 6c,d. Superparamagnetic materials can fluctuate randomly by thermal fluctuation at high enough temperatures just as an atom spin in paramagnetic materials. When the temperature is low, this thermal energy decreases and the magnetic moments are blocked [39]. The temperature below this happens known as blocking temperature which is 290 K as shown in Figure 7. Below the blocking temperature, there is some net alignment of the particle spins, while above it, the spins are in random directions which caused the hysteresis loops to appear at 5 K and increased the magnetic saturation value as shown in Figure 6d and Table 3 [40]. Previous magnetization measurements also indicated that the Fe_3O_4 particles are superparamagnetic at room temperature and ferromagnetic at low temperatures [41]. So, the composites made of Fe_3O_4 particles show similar characteristics.

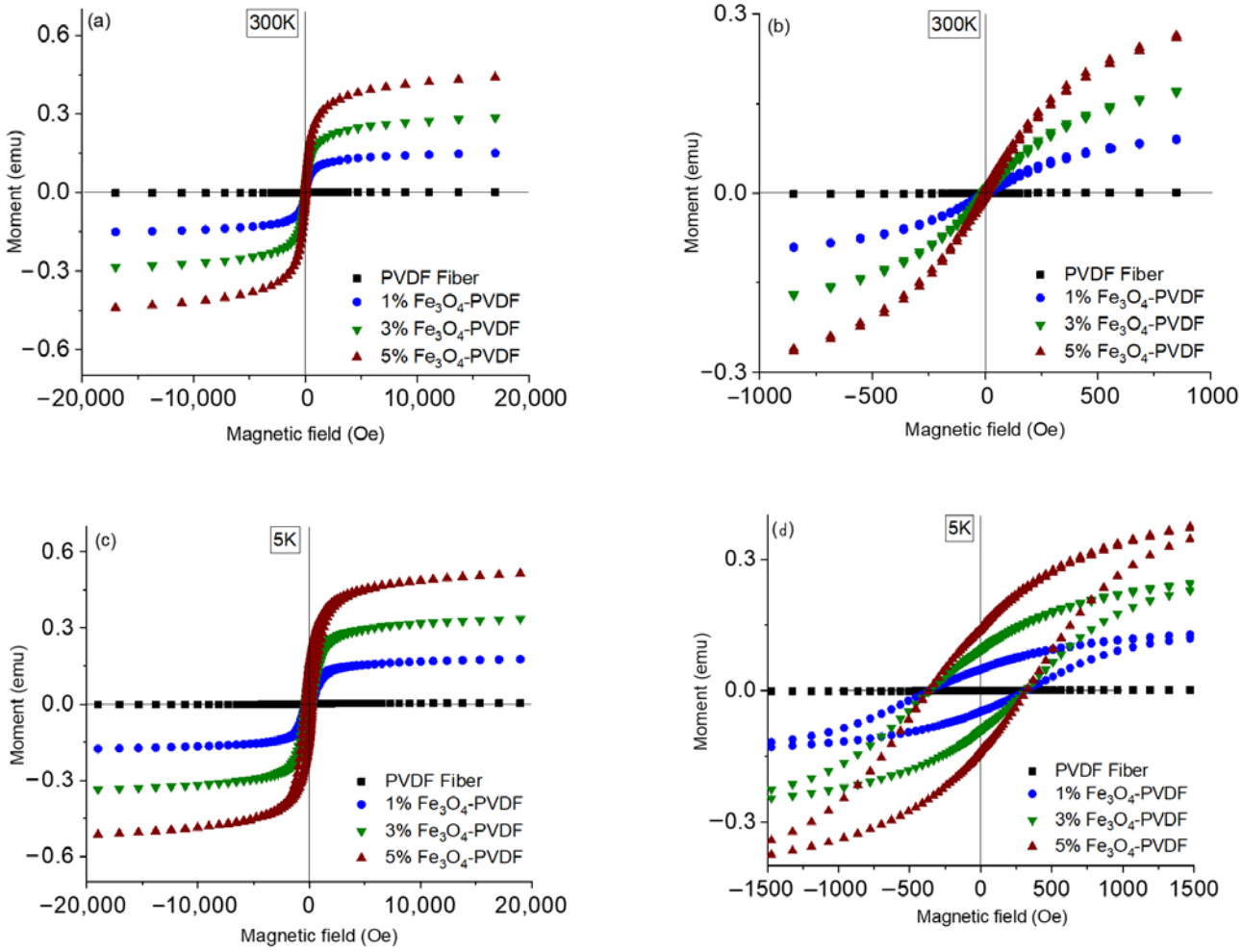

Figure 6. Magnetic hysteresis curves of the samples as a function of the Fe_3O_4 nanoparticles concentration: (**a**) overall response of the samples at 300 K, (**b**) enlarged view of the hysteresis curve around zero field at 300 K, (**c**) overall response of the samples at 5 K, and (**d**) enlarged view of the hysteresis curve around zero field at 5 K.

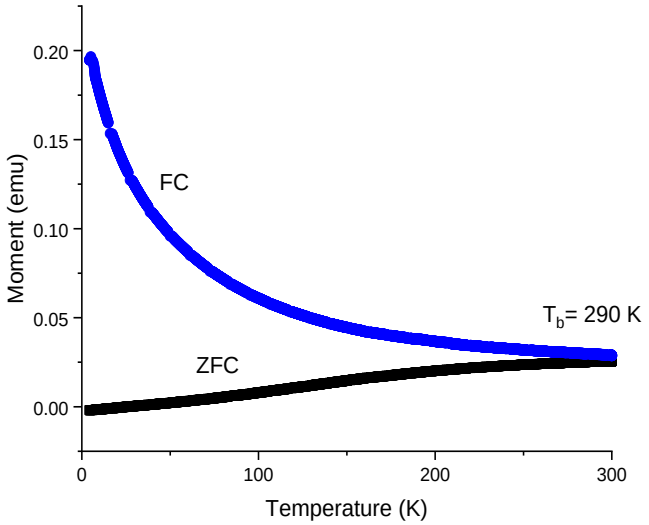

Figure 7. Zero-field-cooled (ZFC) and field-cooled (FC) at 1 T curves for the 5% Fe_3O_4-PVDF.

Table 3. Magnetic saturation values of composite fiber mats at 300 K and 5 K.

Sample	PVDF		1% Fe_3O_4-PVDF		3% Fe_3O_4-PVDF		5% Fe_3O_4-PVDF	
	emu	emu/g	emu	emu/g	emu	emu/g	emu	emu/g
300 K	0	0	0.15	1.28	0.28	3.29	0.44	5.11
5 K	0	0	0.17	1.45	0.33	3.88	0.51	5.93

On the other hand, coercivity measures the resistance of a ferromagnetic material to become demagnetized. A similar coercivity for all the samples in our case indicated that the coercivity is independent of Fe_3O_4 nanoparticles loading, and a homogeneous distribution of nanoparticles in the polymer matrix [42]. PVDF fiber mats did not show any magnetic response at all on both the temperatures but the Fe_3O_4 nanoparticles loaded samples did. With the increase of Fe_3O_4 nanoparticles, the magnetic saturation value of the composites also increased (1.28, 3.29, 5.11 emu/g for 1%, 3% and 5% Fe_3O_4-PVDF respectively) which suggests that ferromagnetic behavior observed in the composites arose from the magnetic Fe_3O_4 nanoparticles.

The magnetic moment vs. temperature (M–T) graph as shown in Figure 7, the separation of zero-field-cooled (ZFC) and field-cooled (FC) curves occur at large temperatures (blocking temperature T_b~290 K) indicating thermal irreversibility of the samples below room temperature. In a superparamagnetic state around 5 K, when the samples were cooled at zero applied field, the magnetic moments were randomly oriented leading to the total magnetization to be around zero as shown in Figure 7. When the temperature started to increase, magnetic moments began to fluctuate, and the presence of an externally applied field aligned them that led to the increase in the magnetization. Similarly, in the case of the field-cooled sample, the magnetic moments were aligned at a higher applied field resulting in higher total magnetization at 5 K starting to decrease with heating. These observations are in agreement with previously reported studies on Fe_3O_4 nanoparticles incorporation in other materials, including ceramic matrices [43].

3.7. Dynamic Mechanical Analyzer (DMA)

To see the stability of the fiber mats, DMA was done for all the samples before and after the magnetization test. Since the magnetization test of fiber mats was done at cryogenic temperature (5 K), it was important to determine their mechanical stability after the test. Dynamic strain sweep was done for all the samples as shown in Figure 8. The Young's modulus (E) calculated from the stress–strain curves are listed in Table 4. The retention of modulus following cryogenic temperature exposure in composite samples over the PVDF

which shows a slight decrease indicates that Fe_3O_4 helped the PVDF matrix to retain its mechanical property after being exposed to cryogenic temperature.

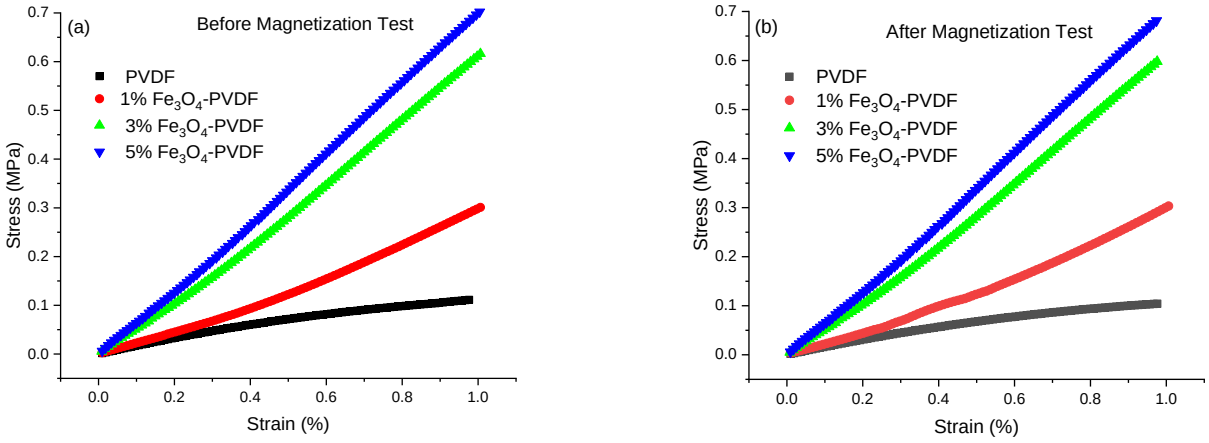

Figure 8. DMA strain sweep curve for composite fiber mats (**a**) before magnetization test and (**b**) after magnetization test at 5 K.

Table 4. Modulus of elasticity (*E*) before and after magnetization test.

Sample	PVDF	1% Fe_3O_4-PVDF	3% Fe_3O_4-PVDF	5% Fe_3O_4-PVDF
E Before magnetization test (MPa)	0.11 ± 0.02	0.30 ± 0.03	0.62 ± 0.03	0.71 ± 0.01
E After magnetization test (MPa)	0.09 ± 0.01	0.29 ± 0.02	0.62± 0.04	0.71 ± 0.03

4. Conclusions

Flexible and mechanically stable PVDF and Fe_3O_4-PVDF composite fiber mats were successfully prepared from one step electrospinning method. A decrease in the fiber diameter was revealed from SEM images as the mass fraction of Fe_3O_4 increased. DSC data suggested that the crystallinity of the composite fiber mats also decreased as a function of Fe_3O_4 concentration in the PVDF matrix. XRD curves identified the reduction in β crystalline phases of the fiber, causing the decrease detected in DSC results. Due to the reduction in the β crystalline phases, the piezoelectric response of the fiber mats dropped by 38% for the maximum Fe_3O_4 loading but that is still 4 times higher than PVDF pellets. The magnetization test advocated a superparamagnetic state of the fiber at room temperature but a ferromagnetic behavior at a lower temperature. The coercivity values of the mats suggested a homogeneous dispersion of the Fe_3O_4 nanoparticles into the PVDF matrix. Moreover, stable and reusable fibers mats were obtained from this process which was confirmed from DMA analysis. The overall results suggest the potential of using Fe_3O_4-PVDF fiber mats as a magnetically responsive textile in spintronics and power electronic devices at cryogenic conditions.

Author Contributions: Conceptualization, N.D.; Data curation, T.C. and D.B.; Formal analysis, T.C. and D.B.; Investigation, T.C.; Methodology, T.C.; Project administration, N.D.; Validation, T.C.; Writing—original draft, T.C.; Writing—review & editing, N.D. and D.B. All authors have read and agreed to the published version of the manuscript.

Funding: This research received no external funding.

Institutional Review Board Statement: Not applicable.

Informed Consent Statement: Not applicable.

Data Availability Statement: The data presented in this study are available within the article.

Acknowledgments: The authors would like to thank Torrance Walker of UNT for visualization work and to the Materials Research Facility (MRF) and Advanced Materials, Manufacturing Processing Institute (AMMPI) for characterization support.

Conflicts of Interest: The authors declare no conflict of interest.

References

1. Zhan, Y.; Long, Z.; Wan, X.; Zhang, J.; He, S.; He, Y. 3D carbon fiber mats/nano-Fe_3O_4 hybrid material with high electromagnetic shielding performance. *Appl. Surf. Sci.* **2018**, *444*, 710–720. [CrossRef]
2. Chiscan, O.; Dumitru, I.; Postolache, P.; Tura, V.; Stancu, A. Electrospun PVC/Fe_3O_4 composite nanofibers for microwave absorption applications. *Mater. Lett.* **2012**, *68*, 251–254. [CrossRef]
3. Honda, H.; Kawabe, A.; Shinkai, M.; Kobayashi, T. Development of chitosan-conjugated magnetite for magnetic cell separation. *J. Ferment. Bioeng.* **1998**, *86*, 191–196. [CrossRef]
4. Lutz, J.-F.; Stiller, S.; Hoth, A.; Kaufner, L.; Pison, U.; Cartier, R. One-Pot Synthesis of PEGylated Ultrasmall Iron-Oxide Nanoparticles and Their In Vivo Evaluation as Magnetic Resonance Imaging Contrast Agents. *Biomacromolecules* **2006**, *7*, 3132–3138. [CrossRef]
5. Pelliccione, M.; Jenkins, A.; Ovartchaiyapong, P.; Reetz, C.; Emmanouilidou, E.; Ni, N.; Jayich, A.C.B. Scanned probe imaging of nanoscale magnetism at cryogenic temperatures with a single-spin quantum sensor. *Nat. Nanotechnol.* **2016**, *11*, 700–705. [CrossRef] [PubMed]
6. Abderrahmane, A.; Ko, P.J.; Okada, H.; Sato, S.-I.; Ohshima, T.; Sandhu, A. Proton irradiation enhancement of low-field negative magnetoresistance sensitivity of AlGaN/GaN-based magnetic sensor at cryogenic temperature. *IEEE Electron Device Lett.* **2014**, *35*, 1130–1132. [CrossRef]
7. Bajpai, O.; Setua, D.; Chattopadhyay, S. A brief overview on ferrite (Fe_3O_4) based polymeric nanocomposites: Recent developments and challenges. *J. Res. Updat. Polym. Sci.* **2014**, *3*, 184.
8. He, F.; Fan, J.; Lau, S. Thermal, mechanical, and dielectric properties of graphite reinforced poly(vinylidene fluoride) composites. *Polym. Test.* **2008**, *27*, 964–970. [CrossRef]
9. An, N.; Liu, H.; Ding, Y.; Zhang, M.; Tang, Y. Preparation and electroactive properties of a PVDF/nano-TiO_2 composite film. *Appl. Surf. Sci.* **2011**, *257*, 3831–3835. [CrossRef]
10. Samadi, A.; Hosseini, S.M.; Mohseni, M. Investigation of the electromagnetic microwaves absorption and piezoelectric properties of electrospun Fe_3O_4-GO/PVDF hybrid nanocomposites. *Org. Electron.* **2018**, *59*, 149–155. [CrossRef]
11. Martins, P.; Lopes, A.C.; Lanceros-Mendez, S. Electroactive phases of poly(vinylidene fluoride): Determination, processing and applications. *Prog. Polym. Sci.* **2014**, *39*, 683–706. [CrossRef]
12. Tasaka, S.; Miyata, S. Effects of crystal structure on piezoelectric and ferroelectric properties of copoly(vinylidenefluoride-tetrafluoroethylene). *J. Appl. Phys.* **1985**, *57*, 906–910. [CrossRef]
13. Ting, Y.; Gunawan, H.; Sugondo, A.; Chiu, C.-W. A New Approach of Polyvinylidene Fluoride (PVDF) Poling Method for Higher Electric Response. *Ferroelectrics* **2013**, *446*, 28–38. [CrossRef]
14. Chowdhury, T.; D'Souza, N.; Dahotre, N. Low-Cost Reliable Corrosion Sensors Using ZnO-PVDF Nanocomposite Textiles. *Sensors* **2021**, *21*, 4147. [CrossRef]
15. Chowdhury, T.; D'Souza, N.; Ho, Y.H.; Dahotre, N.; Mahbub, I. Embedded Corrosion Sensing with ZnO-PVDF Sensor Textiles. *Sensors* **2020**, *20*, 3053. [CrossRef]
16. Mansouri, S.; Sheikholeslami, T.F.; Behzadmehr, A. Investigation on the electrospun PVDF/NP-ZnO nanofibers for application in environmental energy harvesting. *J. Mater. Res. Technol.* **2019**, *8*, 1608–1615. [CrossRef]
17. Ghosal, K.; Chandra, A.; Praveen, G.; Snigdha, S.; Roy, S.; Agatemor, C.; Thomas, S.; Provaznik, I. Electrospinning over Solvent Casting: Tuning of Mechanical Properties of Membranes. *Sci. Rep.* **2018**, *8*, 5058. [CrossRef] [PubMed]
18. Jiang, P.; Lu, J.; Li, K.; Chen, X.; Dan, R. Research on hydrophobicity of electrospun Fe_3O_4/PVDF nanofiber membranes under different preparation conditions. *Full Nanotub. Carbon Nanostruct.* **2019**, *28*, 381–386. [CrossRef]
19. Bhatt, A.S.; Bhat, D.K.; Santosh, M.S. Crystallinity, conductivity, and magnetic properties of PVDF-Fe_3O_4 composite films. *J. Appl. Polym. Sci.* **2010**, *119*, 968–972. [CrossRef]
20. Jayakumar, O.D.; Mandal, B.P.; Majeed, J.; Lawes, G.; Naik, R.; Tyagi, A.K. Inorganic–organic multiferroic hybrid films of Fe_3O_4 and PVDF with significant magneto-dielectric coupling. *J. Mater. Chem. C* **2013**, *1*, 3710–3715. [CrossRef]
21. Prabhakaran, T.; Hemalatha, J. Ferroelectric and magnetic studies on unpoled (*Polyvinylidine fluoride*)/Fe_3O_4 magnetoelectric nanocomposite structures. *Mater. Chem. Phys.* **2013**, *137*, 781–787. [CrossRef]
22. Huang, Z.-Q.; Zheng, F.; Zhang, Z.; Xu, H.-T.; Zhou, K.-M. The performance of the PVDF-Fe_3O_4 ultrafiltration membrane and the effect of a parallel magnetic field used during the membrane formation. *Desalination* **2012**, *292*, 64–72. [CrossRef]
23. Chen, D.; Li, J.; Yuan, Y.; Gao, C.; Cui, Y.; Li, S.; Liu, X.; Wang, H.; Peng, C.; Wu, Z. A Review of the Polymer for Cryogenic Application: Methods, Mechanisms and Perspectives. *Polymers* **2021**, *13*, 320. [CrossRef]
24. He, Y.; Chen, Q.; Yang, S.; Lu, C.; Feng, M.; Jiang, Y.; Cao, G.; Zhang, J.; Liu, C. Micro-crack behavior of carbon fiber reinforced Fe_3O_4/graphene oxide modified epoxy composites for cryogenic application. *Compos. Part A Appl. Sci. Manuf.* **2018**, *108*, 12–22. [CrossRef]

25. Zhang, C.C.; Li, X.; Yang, Y.; Wang, C. Polymethylmethacrylate/Fe_3O_4 composite nanofiber membranes with ultra-low dielectric permittivity. *Appl. Phys. A* **2009**, *97*, 281–285. [CrossRef]
26. Sorayani-Bafqi, M.S.; Bagherzadeh, R.; Latifi, M. Fabrication of composite PVDF-ZnO nanofiber mats by electrospinning for energy scavenging application with enhanced efficiency. *J. Polym. Res.* **2015**, *22*, 130. [CrossRef]
27. Xu, C.; Ouyang, C.; Jia, R.; Li, Y.; Wang, X. Magnetic and optical properties of poly(vinylidene difluoride)/Fe_3O_4 nanocomposite prepared by coprecipitation approach. *J. Appl. Polym. Sci.* **2009**, *111*, 1763–1768. [CrossRef]
28. Croce, F.; Appetecchi, G.B.; Persi, L.; Scrosati, B. Nanocomposite polymer electrolytes for lithium batteries. *Nat. Cell Biol.* **1998**, *394*, 456–458. [CrossRef]
29. Gang, W.; Roos, J.; Brinkmann, D.; Capuano, F.; Croce, F.; Scrosati, B. Comparison of NMR and conductivity in $(PEP)_8LiClO_4$+γ-$LiAlO_2$. *Solid State Ion.* **1992**, *53*, 1102–1105. [CrossRef]
30. Chu, P.P.; Reddy, M.J. Sm_2O_3 composite PEO solid polymer electrolyte. *J. Power Sources* **2003**, *115*, 288–294. [CrossRef]
31. Weston, J.; Steele, B. Effects of inert fillers on the mechanical and electrochemical properties of lithium salt-poly(ethylene oxide) polymer electrolytes. *Solid State Ion.* **1982**, *7*, 75–79. [CrossRef]
32. Wieczorek, W.; Such, K.; Wyciślik, H.; Płocharski, J. Modifications of crystalline structure of PEO polymer electrolytes with ceramic additives. *Solid State Ion.* **1989**, *36*, 255–257. [CrossRef]
33. Sukitpaneenit, P.; Chung, T.-S. Molecular elucidation of morphology and mechanical properties of PVDF hollow fiber mem-branes from aspects of phase inversion, crystallization and rheology. *J. Membr. Sci.* **2009**, *340*, 192–205. [CrossRef]
34. Leo, C.J.; Thakur, A.K.; Subba-Rao, G.V.; Chowdari, B.V.R. Effect of glass—Ceramic filler on properties of polyethylene oxide–$LiCF_3SO_3$ complex. *J. Power Sources* **2003**, *115*, 295–304. [CrossRef]
35. Kim, M.; Wu, Y.; Kan, E.; Fan, J. Breathable and Flexible Piezoelectric ZnO@PVDF Fibrous Nanogenerator for Wearable Applications. *Polymers* **2018**, *10*, 745. [CrossRef] [PubMed]
36. Bormashenko, E.; Pogreb, R.; Stanevsky, O. Vibrational spectrum of PVDF and its interpretation. *Polym. Test.* **2004**, *23*, 791–796. [CrossRef]
37. Salimi, A.; Yousefi, A.A. Analysis Method: FTIR studies of β-phase crystal formation in stretched PVDF films. *Polym. Test.* **2003**, *22*, 699–704. [CrossRef]
38. Zhao, P.; Wang, S.; Kadlec, A. Piezoelectric and dielectric properties of nanoporous polyvinylidence fluoride (PVDF) films. *Behav. Mech. Multifunct. Mater. Compos.* **2016**, *9800*, 98000. [CrossRef]
39. Goya, G.; Morales, M.D.P. Field Dependence of Blocking Temperature in Magnetite Nanoparticles. *J. Metastab. Nanocryst. Mater.* **2004**, *20–21*, 673–678. [CrossRef]
40. Sara-Majetich, T.W.; Mefford, O.T. Magnetic Nanoparticles. *MRS Bull.* **2013**, *38*, 899–903. [CrossRef]
41. Demir, A.; Topkaya, R.; Baykal, A. Green synthesis of superparamagnetic Fe_3O_4 nanoparticles with maltose: Its magnetic investigation. *Polyhedron* **2013**, *65*, 282–287. [CrossRef]
42. Ramajo, L.A.; Cristóbal, A.A.; Botta, P.M.; Porto-López, J.M.; Reboredo, M.M.; Castro, M.S. Dielectric and magnetic response of Fe_3O_4/epoxy composites. *Compos. Part A Appl. Sci. Manuf.* **2009**, *40*, 388–393. [CrossRef]
43. Berman, D.; Sha, Y.; Shevchenko, E. Effect of Polymer Removal on the Morphology and Phase of the Nanoparticles in All-Inorganic Heterostructures Synthesized via Two-Step Polymer Infiltration. *Molecules* **2021**, *26*, 679. [CrossRef] [PubMed]